

Quantum dynamics of collective spin states in a thermal gasRoy Shaham,^{1,2,*} Or Katz,^{1,2} and Ofer Firstenberg¹¹*Department of Physics of Complex Systems, Weizmann Institute of Science, Rehovot 76100, Israel*²*Rafael, Ltd., IL-31021 Haifa, Israel*

(Received 7 June 2020; accepted 7 July 2020; published 30 July 2020)

Ensembles of alkali-metal or noble-gas atoms at room temperature and above are widely applied in quantum optics and metrology owing to their long-lived spins. Their collective spin states maintain nonclassical nonlocal correlations, despite the atomic thermal motion in the bulk and at the boundaries. Here we present a stochastic, fully quantum description of the effect of atomic diffusion in these systems. We employ the Bloch-Heisenberg-Langevin formalism to account for the quantum noise originating from diffusion and from various boundary conditions corresponding to typical wall coatings, thus modeling the dynamics of nonclassical spin states with spatial interatomic correlations. As examples, we apply the model to calculate spin noise spectroscopy, temporal relaxation of squeezed spin states, and the coherent coupling between two spin species in a hybrid system.

DOI: [10.1103/PhysRevA.102.012822](https://doi.org/10.1103/PhysRevA.102.012822)**I. INTRODUCTION**

Gaseous spin ensembles operating at room temperature and above have attracted much interest for decades. At ambient conditions, alkali-metal vapors and odd isotopes of noble gases exhibit long spin-coherence times, ranging from milliseconds to hours [1–6]. These spin ensembles, consisting of a macroscopic number of atoms, are beneficial for precision sensing, searches of new physics, and demonstration of macroscopic quantum effects [7–13]. In particular, manipulations of collective spin states allow for demonstrations of basic quantum phenomena, including entanglement, squeezing, and teleportation [14–17] as well as storage and generation of photons [18–21]. It is the collectively enhanced coupling and the relatively low noise offered by these spin ensembles that make them particularly suitable for metrology and quantum information applications.

Thermal atomic motion is an intrinsic property of the dynamics in gaseous systems. Gas-phase atoms, in low-pressure room-temperature systems, move at hundreds of meters per second in ballistic trajectories, crossing the cell at submillisecond timescales and interacting with its boundaries. To suppress wall collisions, buffer gas is often introduced, which renders the atomic motion diffusive via velocity-changing collisions [22]. At the theory level, the effect of diffusion on the mean spin has been extensively addressed, essentially by describing the evolution of an impure (mixed) spin state in the cell using a mean-field approximation [23–28]. This common formalism treats the spatial dynamics of an average atom in any given position using a spatially dependent density matrix. It accurately captures the single-atom dynamics but neglects both interatomic correlations and thermal fluctuations associated with the spin motion and collisions.

Nonclassical phenomena involving collective spin states, such as transfer of quantum correlations between nonoverlap-

ping light beams by atomic motion [29–31], call for a quantum description of the thermal motion. For spin-exchange collisions, which are an outcome of thermal motion, such a quantum description has received much recent attention [32–39]. However, the more direct consequences of thermal motion, namely, the stochasticity of the spatial dynamics in the bulk and at the system's boundaries, still lack a proper fully quantum description.

In this paper, we describe the effect of spatial diffusion on the quantum state of warm spin gases. Using the Bloch-Heisenberg-Langevin formalism, we identify the dissipation and noise associated with atomic thermal motion and with the scattering off the cell boundaries. Existing significant work in this field relies primarily on mean-field models, which address both wall coupling [40] and diffusion in unconfined systems [41]. The latter work derives the correlation function of diffusion-induced quantum noise from the correlation function of mass diffusion in unconfined systems. Here we derive the quantum noise straight out of Brownian motion considerations and provide a solution for confined geometries. Our model generalizes the mean-field results and enables the description of interatomic correlations and collective quantum states of the ensemble. We apply the model to highly polarized spin vapor and analyze the effect of diffusion in various conditions, including spin noise (SN) spectroscopy [12,42–46], spin squeezing [14,32], and coupling of alkali-metal to noble-gas spins in the strong-coupling regime [33,34].

The paper is arranged as follows. We derive in Sec. II the Bloch-Heisenberg-Langevin model for the evolution of the collective spin operator due to atomic Brownian motion and cell boundaries. We focus on highly polarized ensembles in Sec. III and provide the model solutions. In Sec. IV, we present several applications of our model. We discuss how it is employed to describe the temporal evolution, to calculate experimental results, to provide insight, and to optimize setups for specific tasks. Limits of our model and differences from existing models, as well as future prospects, are discussed in Sec. V. We provide appendices that elaborate on the quantum

*roy.shaham@weizmann.ac.il

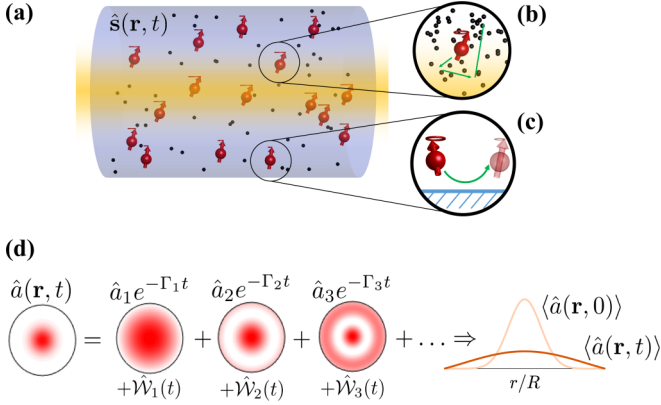


FIG. 1. (a) Atomic spins in the gas phase, comprising a collective quantum spin $\hat{\mathbf{s}}(\mathbf{r}, t)$ and undergoing thermal motion. (b) In the diffusive regime, the spins spatially redistribute via frequent velocity-changing collisions. (c) Collisions (local interaction) with the walls of the gas cell may fully or partially depolarize the spin state. (d) Diffusion and wall collisions lead to a multimode evolution, here exemplified for a spin excitation $\hat{a}(\mathbf{r}, t) \propto \hat{s}_x(\mathbf{r}, t) - i\hat{s}_y(\mathbf{r}, t)$ with an initial Gaussian-like spatial distribution $\langle \hat{a}(\mathbf{r}, t) \rangle$ and for destructive wall collisions. In addition to the mode-specific decay Γ_n , each spatial mode accumulates mode-specific quantum noise $\hat{\mathcal{W}}_n(t)$.

noise produced by thermal motion (Appendix A), a simplified model for analyzing the scattering off the cell walls (Appendix B), means of solving the Bloch-Heisenberg-Langevin equation (Appendix C), and the Faraday rotation scheme used herein (Appendix D).

II. MODEL

Consider a warm ensemble of N_a atomic spins confined in a cell, as illustrated in Fig. 1(a). Let $\mathbf{r}_a(t)$ be the classical location of the a th atom at time t and define the single-body density function at some location \mathbf{r} as $n_a(\mathbf{r}) = \delta[\mathbf{r} - \mathbf{r}_a(t)]$. We denote the spin operator of the a th atom by $\hat{\mathbf{s}}_a$ and define the space-dependent collective spin operator as $\hat{\mathbf{s}}(\mathbf{r}, t) = \sum_{a=1}^{N_a} \hat{\mathbf{s}}_a n_a(\mathbf{r})$. While formally $\hat{\mathbf{s}}(\mathbf{r}, t)$ is sparse and spiked, practical experiments address only its coarse-grained properties, e.g., due to finite spatial scale of the employed optical or magnetic fields. The time evolution of the collective spin operator is given by

$$\frac{\partial \hat{\mathbf{s}}}{\partial t} = \sum_{a=1}^{N_a} \frac{\partial \hat{\mathbf{s}}_a}{\partial t} n_a + \hat{\mathbf{s}}_a \frac{\partial n_a}{\partial t}. \quad (1)$$

Here the first term accounts for the internal degrees of freedom, including the local Hamiltonian evolution of the spins and spin-spin interactions, while the second term accounts for the external degrees of freedom, namely, for motional effects. The focus of this paper is on the second term, considered in the diffusion regime as illustrated in Fig. 1(b). We consider the first term only for its contribution to the boundary conditions, via the effect of wall collisions as illustrated in Fig. 1(c). In the following, we first derive the equations governing the quantum operator $\hat{\mathbf{s}}(\mathbf{r}, t)$ in the bulk and subsequently introduce the effect of the boundaries.

A. Diffusion in the bulk

We consider the limit of gas-phase atoms experiencing frequent, spin-preserving, velocity-changing collisions, such as those characterizing a dilute alkali-metal vapor in an inert buffer gas. In this so-called Fickian diffusion regime, the atomic motion is diffusive, and the local density evolution can be described by the stochastic differential equation [47]

$$\partial n_a / \partial t = D \nabla^2 n_a + \nabla (\boldsymbol{\eta} \sqrt{n_a}), \quad (2)$$

where D is the diffusion coefficient, and $\boldsymbol{\eta}$ is a white Gaussian stochastic process the components of which satisfy $\langle \eta_i(\mathbf{r}, t) \eta_j(\mathbf{r}', t') \rangle_c = 2D \delta_{ij} \delta(\mathbf{r} - \mathbf{r}') \delta(t - t')$ for $i, j = x, y, z$. We use $\langle \cdot \rangle_c$ to represent ensemble average over the classical atomic trajectories, differing from the quantum expectation value $\langle \cdot \rangle$. The first term in Eq. (2) leads to delocalization of the atomic position via deterministic diffusion, while the second term introduces fluctuations that localize the atoms to discrete positions. Equation (2), derived by Dean for Brownian motion in the absence of long-range interactions [47], is valid under the coarse-grain approximation, when the temporal and spatial resolutions are coarser than the mean free time and path between collisions.

Substituting $\partial n_a / \partial t$ into Eq. (1), we obtain the Bloch-Heisenberg-Langevin dynamical equation for the collective spin:

$$\partial \hat{\mathbf{s}} / \partial t = i[\mathcal{H}, \hat{\mathbf{s}}] + D \nabla^2 \hat{\mathbf{s}} + \hat{\mathbf{f}}. \quad (3)$$

Here \mathcal{H} is the spin Hamiltonian in the absence of atomic motion, originating from the $\partial \hat{\mathbf{s}}_a / \partial t$ term in Eq. (1). The quantum noise operator $\hat{\mathbf{f}} = \hat{\mathbf{f}}(\mathbf{r}, t)$ is associated with the local fluctuations of the atomic positions. It can be formally written as $\hat{f}_\mu = \nabla (\hat{s}_\mu \boldsymbol{\eta} / \sqrt{n})$, where $\mu = x, y, z$, and $n = \sum_a n_a$ is the atomic density. The noise term has an important role in preserving the mean spin moments of the ensemble. The commutation relation of different instances of the noise $\hat{f}_\mu = \hat{f}_\mu(\mathbf{r}, t)$ and $\hat{f}'_\nu = \hat{f}'_\nu(\mathbf{r}', t')$ satisfies

$$\langle [\hat{f}_\mu, \hat{f}'_\nu] \rangle_c = 2i \epsilon_{\xi\mu\nu} D (\nabla \nabla') \hat{s}_\xi \delta(\mathbf{r} - \mathbf{r}') \delta(t - t'), \quad (4)$$

where $\epsilon_{\xi\mu\nu}$ is the Levi-Civita antisymmetric tensor. These commutation relations ensure the conservation of spin commutation relations $[\hat{s}_\mu(\mathbf{r}, t), \hat{s}_\nu(\mathbf{r}', t)] = i \epsilon_{\xi\mu\nu} \hat{s}_\xi \delta(\mathbf{r} - \mathbf{r}')$ on the operator level, compensating for the diffusion-induced decay in the bulk due to the $D \nabla^2$ term. We provide the full derivation of $\hat{\mathbf{f}}$ and its properties in Appendix A.

The spin noise process is temporally white and spatially colored, with higher noise content for shorter wavelengths. The increase of noise at a fine-grain scale counteracts the diffusion term, which decreases the spin variations faster at smaller length scales; this is a manifestation of the fluctuation-dissipation theorem. Finally, as expected, ensemble averaging over the noise realizations leaves only the diffusion term in the mean-field Bloch equation for the spin $\partial \langle \mathbf{s} \rangle / \partial t = D \nabla^2 \langle \mathbf{s} \rangle$, where $\langle \mathbf{s} \rangle = \langle \hat{\mathbf{s}}(\mathbf{r}, t) \rangle$ is the spin expectation value at a coarse-grained position \mathbf{r} .

B. Boundary conditions

We now turn to derive the contribution of wall collision to the quantum dynamics of the collective spin. When the

atoms diffuse to the boundaries of the cell, their spin interacts with the surface of the walls. This interaction plays an important role in determining the depolarization and decoherence times of the total spin [7,22] and may also induce frequency shifts [24,48–51]. Bare glass strongly depolarizes alkali-metal atoms, and magnetic impurities in the glass affect the nuclear spin of noble-gas atoms. To attenuate the depolarization at the walls, cells can be coated with spin-preserving coatings such as paraffin [4,52,53] or octadecyltrichlorosilane (OTS) [40] for alkali-metal vapor and Surfasil or SolGel [54–57] for spin-polarized xenon. The coupling between the spins and the cell walls constitutes the formal boundary conditions of Eq. (3).

In the mean-field picture, the wall coupling can be described as a local scatterer for the spin-density matrix ρ . In this picture, assisted by kinetic gas theory, the boundary conditions can be written as [23]

$$(1 + \frac{2}{3}\lambda\hat{\mathbf{n}} \cdot \nabla)\rho = (1 - \frac{2}{3}\lambda\hat{\mathbf{n}} \cdot \nabla)\mathcal{S}\rho, \quad (5)$$

where \mathcal{S} is the wall scattering matrix. Here λ denotes the mean free path of the atoms, related to the diffusion coefficient via $D = \lambda\bar{v}/3$, where \bar{v} is the mean thermal velocity.

We adopt a similar perspective in order to derive the coupling of the collective spin $\hat{\mathbf{s}}$ with the walls in the Bloch-Heisenberg-Langevin formalism. In this formalism, the scattering off the walls introduces not only decay, but also fluctuations. In the Markovian limit, when each scattering event is short, its operation on a single spin becomes a stochastic density matrix:

$$\mathcal{S}\hat{\mathbf{s}}_a = e^{-1/N}\hat{\mathbf{s}}_a + \hat{\mathbf{w}}_a. \quad (6)$$

Here N denotes the average number of wall collisions a spin withstands before depolarizing [40]. The accompanied quantum noise process is $\hat{\mathbf{w}}_a$; it ensures the conservation of spin commutation relations at the boundary.

Using the stochastic scattering matrix, we generalize the mean-field boundary condition [Eq. (5)] for collective spin operators as

$$(1 - e^{-1/N})\hat{\mathbf{s}} + \frac{2}{3}\lambda(1 + e^{-1/N})(\hat{\mathbf{n}} \cdot \nabla)\hat{\mathbf{s}} = \hat{\mathbf{w}}. \quad (7)$$

Here $\hat{\mathbf{w}}(\mathbf{r}, t) = \sum_a \hat{\mathbf{w}}_a n_a$, for positions \mathbf{r} on the cell boundary, is the collective wall-coupling noise process affecting the local spin on the wall. $\hat{\mathbf{w}}$ is zero on average and its statistical properties, together with the derivation of Eq. (6), are discussed in Appendix B. The first term in Eq. (7) describes the fractional depolarization by the walls, and the second term describes the difference between the spin flux entering and exiting the wall. If the wall coupling also includes a coherent frequency-shift component, it can be appropriately added to these terms. The term on the right-hand side describes the associated white fluctuations.

In the limit of perfect spin-preserving coating, the boundary condition becomes a no-flux (Neumann) condition satisfying $(\hat{\mathbf{n}} \cdot \nabla)\hat{\mathbf{s}} = 0$, and depolarization is minimized. This limit is realized for $N \gg R/\lambda$, where R is the dimension of the cell [58] [7]. In the opposite limit of strongly depolarizing walls, i.e., $N \lesssim 1$, the (Dirichlet) boundary condition is $\hat{\mathbf{s}} = \hat{\mathbf{w}}/(1 - e^{-1/N})$ [59], rendering the scattered spin state random. For any other value of N (partially depolarizing walls), the

boundary condition in Eq. (7) is identified as a stochastic Robin boundary condition [60].

The two mechanisms discussed in this section—the bulk diffusion and the wall coupling—are independent physical processes. This is evident by the different parameters characterizing them— D and N —which are dictated by different physical scales, such as buffer gas pressure and the quality of the wall coating. These processes are different in nature; while wall coupling leads to spin depolarization and thermalization, diffusion leads to spin redistribution while conserving the total spin. They introduce independent fluctuations and dissipation, and they affect the spins at different spatial domains (the bulk and the boundary). That being said, both processes are necessary to describe the complete spin dynamics in a confined volume, simultaneously satisfying Eqs. (3) and (7).

III. POLARIZED ENSEMBLES

When discussing nonclassical spin states for typical applications, it is beneficial to consider the prevailing limit of highly polarized ensembles. Let us assume that most of the spins point downwards ($-\hat{\mathbf{z}}$). In this limit, we follow the Holstein-Primakoff transformation [61,62] and approximate the longitudinal spin component by its mean value $\hat{s}_z(\mathbf{r}, t) = s_z$ (with $s_z = -n/2$ for spin $1/2$). The ladder operator $\hat{s}_- = \hat{s}_x - i\hat{s}_y$, which flips a single spin downwards at position \mathbf{r} , can be represented by the annihilation operator $\hat{a} = \hat{s}_-/\sqrt{2|s_z|}$. This operator satisfies the bosonic commutation relations $[\hat{a}(\mathbf{r}, t), \hat{a}^\dagger(\mathbf{r}', t)] = \delta(\mathbf{r} - \mathbf{r}')$. Under these transformations, Eqs. (3) and (7) become

$$\partial\hat{a}/\partial t = i[\mathcal{H}, \hat{a}] + D\nabla^2\hat{a} + \hat{f}, \quad (8)$$

$$(1 - e^{-1/N})\hat{a} = -\frac{2}{3}\lambda(1 + e^{-1/N})\hat{\mathbf{n}} \cdot \nabla\hat{a} + \hat{w}, \quad (9)$$

where both $\hat{f} = (\hat{f}_x - i\hat{f}_y)/\sqrt{2|s_z|}$ and $\hat{w} = (\hat{w}_x + i\hat{w}_y)/\sqrt{2|s_z|}$ are now vacuum noise processes (see Appendices A and B; note that \hat{f} is spatially colored). Here, Eq. (8) describes the spin dynamics in the bulk, while Eq. (9) holds at the boundary.

We solve Eqs. (8) and (9) by decomposing the operators into a superposition of nonlocal diffusion modes $\hat{a}(\mathbf{r}, t) = \sum_n \hat{a}_n(t)u_n(\mathbf{r})$. We first identify the mode functions $u_n(\mathbf{r})$ by solving the homogeneous Helmholtz equation $(D\nabla^2 + \Gamma_n)u_n(\mathbf{r}) = 0$, where the eigenvalues $-\Gamma_n$ are fixed by the Robin boundary condition [Eq. (9) without the noise term]. The operator $\hat{a}_n(t) = \int_V \hat{a}(\mathbf{r}, t)u_n^*(\mathbf{r})d^3\mathbf{r}$, where V is the cell volume, annihilates a collective transverse spin excitation with a nonlocal distribution $|u_n(\mathbf{r})|^2$ and a relaxation rate Γ_n . These operators satisfy the bosonic commutation relation $[\hat{a}_n, \hat{a}_m^\dagger] = \delta_{nm}$. The noise terms \hat{f} and \hat{w} are decomposed using the same mode-function basis. This leads to mode-specific noise terms $\hat{\mathcal{W}}_n(t)$, operating as independent sources.

Assuming, for the sake of example, a magnetic (Zeeman) Hamiltonian $\mathcal{H} = \omega_0\hat{s}_z$, where ω_0 is the Larmor precession frequency around a $\hat{\mathbf{z}}$ magnetic field, the time evolution of the mode operators is given by

$$\hat{a}_n(t) = \hat{a}_n(0)e^{-i(\omega_0 + \Gamma_n)t} + \hat{\mathcal{W}}_n(t). \quad (10)$$

TABLE I. Solutions of the diffusion-relaxation modes for rectangular, cylindrical, and spherical cells. $J_n(x)$ is the n th Bessel function of the first kind, $j_\ell(x)$ is the ℓ th spherical Bessel function of the first kind, and $Y_{\ell p}(\theta, \varphi)$ are the spherical harmonics. The decay rates satisfy $\Gamma_n = Dk_n^2$.

Cell shape	Rectangular	Cylindrical	Spherical
Symmetry	Symmetric: (+) Antisymmetric: (-)	Angular: n	Spherical: ℓ, p
Coordinate range	$-L/2 \leq x \leq L/2$	$0 \leq \rho \leq R$ $0 \leq \varphi \leq 2\pi$	$0 \leq r \leq R$ $0 \leq \theta \leq \pi$ $0 \leq \varphi \leq 2\pi$
Boundary equation	$\cot(k_n^+ L/2) = \frac{2}{3} \frac{1+e^{-1/N}}{1-e^{-1/N}} \lambda k_n^+$ $-\tan(k_n^- L/2) = \frac{2}{3} \frac{1+e^{-1/N}}{1-e^{-1/N}} \lambda k_n^-$	$-\frac{J_n(k_{vn}R)}{J_n'(k_{vn}R)} = \frac{2}{3} \frac{1+e^{-1/N}}{1-e^{-1/N}} \lambda k_{vn}$	$-\frac{j_\ell(k_{n\ell}R)}{j_\ell'(k_{n\ell}R)} = \frac{2}{3} \frac{1+e^{-1/N}}{1-e^{-1/N}} \lambda k_{n\ell}$
$u_n(\mathbf{r})$	$u_n^+(x) = A_n^+ \cos(k_n^+ x)$ $u_n^-(x) = A_n^- \sin(k_n^- x)$	$u_{vn}(\rho, \varphi) = A_{vn} J_n(k_{vn} \rho) e^{in\varphi}$	$u_{n\ell p}(r, \theta, \varphi) = A_{n\ell p} j_\ell(k_{n\ell} r) Y_{\ell p}(\theta, \varphi)$

The multimode decomposition and evolution are illustrated in Fig. 1(d), showing the first angular-symmetric mode distributions $u_n(\mathbf{r})$ of a cylindrical cell. In Table I, we provide explicit solutions of the mode bases and associated decay rates for any given boundary properties in either rectangular, cylindrical, or spherical cells. The solution procedure and the corresponding decomposition of the noise terms are demonstrated for an exemplary one-dimensional (1D) geometry in Appendix C. We note that, asymptotically, the decay of high-order modes ($n \gg 1$) is independent of cell geometry and is approximately given by $\Gamma_n \sim D(\pi n V^{-1/3})^2$, where $\pi n V^{-1/3}$ approximates the mode's wave number.

IV. APPLICATIONS

The outlined Bloch-Heisenberg-Langevin formalism applies to various experimental configurations and applications. It should be particularly useful when two constituents of the same system have different spatial characteristics, leading to different spatial modes. That occurs, for example, when coupling spins to optical fields [Fig. 1(d)] or when mixing atomic species with different wall couplings. In this section, we consider three such relevant, real-life cases.

A. Spin noise spectroscopy

SNS allows one to extract physical data out of the noise properties of the spin system. It is used for magnetometry with atomic ensembles in or out of equilibrium [12,43,44,46,63], for low-field NMR [64], for fundamental noise studies aimed at increasing metrological sensitivity [9,12], and more [42]. SNS is also used to quantify interatomic correlations in squeezed states, when it is performed with precision surpassing the standard quantum limit [14,32,39,43].

Spin noise in an alkali-metal vapor is affected by various dephasing mechanisms. Here we describe the effect of diffusion, given a spatially fixed light beam employed to probe the spins. Since this probe beam may overlap with several spatial modes of diffusion, the measured noise spectrum would depend on the beam size, cell dimensions, and diffusion characteristics. On the mean-field level, this effect has been described by motion of atoms in and out of the beam [28,65]. Here we calculate the SNS directly out of the quantum noise induced by the thermal motion as derived above.

For concreteness, we consider two cylindrical cells of radius $R = 1$ cm and length $L = 3$ cm. One cell contains 100 Torr of buffer gas, providing for $\lambda = 0.5 \mu\text{m}$ and $D = 1 \text{ cm}^2/\text{s}$, and no spin-preserving coating $N \lesssim 1$ (e.g., as in Ref. [32]). The other cell has a high-quality paraffin coating, allowing for $N = 10^6$ wall collisions before depolarization [4], and only dilute buffer gas originating from outgassing of the coating, such that $\lambda = 1 \text{ mm}$ and $D = 3 \times 10^3 \text{ cm}^2/\text{s}$ rendering the atomic motion in the Fickian regime ($\lambda \ll R, L$) [66,67]. A probe beam with waist radius w_0 measures the alkali-metal spin \hat{x} component, oriented along the cylinder axis as presented in Fig. 2(a). The cell is placed inside a magnetic field $\mathbf{B} = 2\pi f_0/g_a \cdot \hat{z}$ pointing along the spin polarization, where g_a is the alkali-metal gyromagnetic ratio.

In Appendix D, we review the measurement details and calculate the spin noise spectral density $S_{xx}(f)$ for both cells:

$$S_{xx}(f) = \sum_n \frac{|I_n^{(G)}|^2}{4} \frac{2\tilde{P}\Gamma_n}{\Gamma_n^2 + 4\pi^2(f - f_0)^2}, \quad (11)$$

where f is the frequency in which the SNS is examined, Γ_n is again the decay rate of the n th diffusion mode, $I_n^{(G)}$ is the overlap of the Gaussian probe beam with that mode, and \tilde{P} depends on the spin statistics and on the polarization, such that $\tilde{P} = 1$ for highly polarized ensembles and for spin 1/2.

The calculated spectra are shown in Figs. 2(b) and 2(c) for $w_0 = 1$ mm. The cusplike spectra originate from a sum of Lorentzians, the relative weights of which correspond to the overlap of the probe beam with each given mode $|I_n^{(G)}|^2$. In the past, this cusp was identified as a universal phenomena [65], while here we recreate this result using the eigenmodes and accounting for the boundary. With spin-preserving coating, the uniform mode $n = 0$ decays slower, and its contribution to the noise spectrum is much more pronounced, while the higher-order modes decay faster due to lack of buffer gas.

The dominance of the central narrow feature thus depends on the overlap of the probe with the least-decaying mode $|I_0^{(G)}|^2$. To quantify it, we define the unitless noise content $\zeta = \int_{-f_{1/2}}^{f_{1/2}} S_{xx}(f) df$ as the fraction of the noise residing within the full width at half maximum of the spectrum. Figure 2(d) shows ζ for different beam sizes w_0/R . Evidently, the spin resonance is more significant in the buffer gas cell, unless the probe beam covers the entire cell. This should be an important consideration in the design of such experiments.

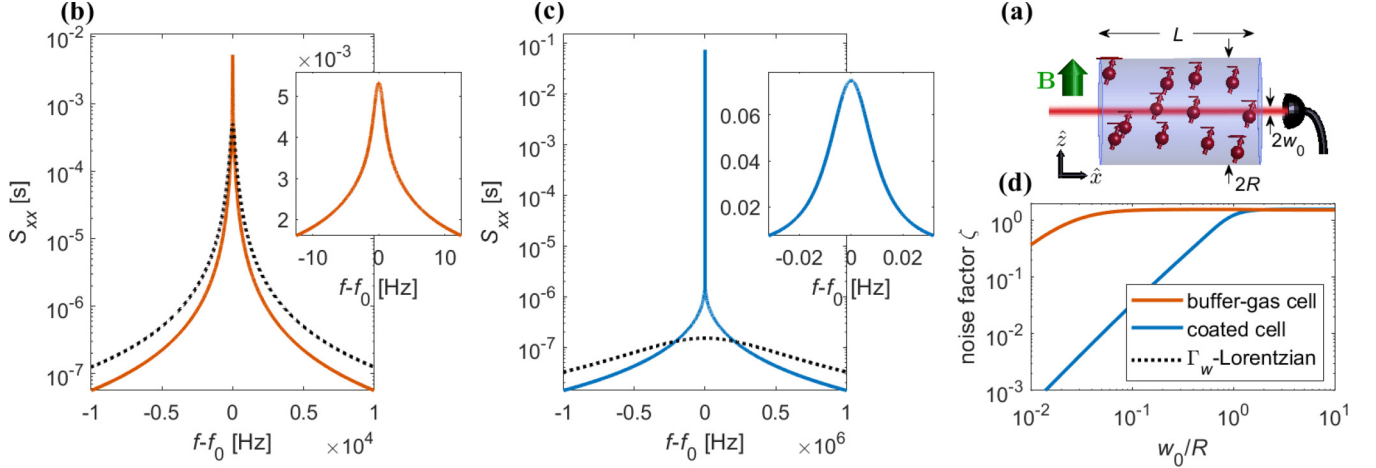


FIG. 2. Effect of thermal motion in spin noise spectroscopy. (a) The spins are initially polarized along a magnetic field $B\hat{z}$, and the spin projection (\hat{s}_x) is measured by Faraday rotation using a nondiverging Gaussian probe beam. The calculation assumes a probe waist radius of $w_0 = 1$ mm and a cylindrical cell with radius $R = 1$ cm and length $L = 3$ cm. (b) Spin noise spectrum for an uncoated cell with a dense buffer gas ($D = 1$ cm²/s, $N \leq 1$), calculated using Eq. (11). Many spatial (diffusion) modes contribute to the noise, and thus the total signal is a weighted sum of varying Lorentzians, producing a cusp profile. (c) Spin noise spectrum for a cell coated with high-quality paraffin coating ($D = 3 \times 10^3$ cm²/s, $N = 10^6$). The cusp is wider (since D is larger), except for an additional sharp feature associated with the uniform spatial mode, the slow decay of which is governed by wall collisions. The dotted lines in (b) and (c) are a simple Lorentzian with width $\Gamma_w = \pi^2 D/w_0^2$, provided as reference for a single-mode approximation. (d) Noise content in the vicinity of the resonance (as defined in the main text) for the same two cells and varying probe waists. The narrower the probe beam, the larger its overlap with the high-order, rapidly decaying, diffusion modes, thus leading to weaker signal in the central resonance feature. This effect becomes more pronounced for lower buffer gas pressures.

B. Squeezed-state lifetime

When the spin noise is measured with a sensitivity below the standard quantum limit, the spin ensemble is projected into a collective squeezed spin state. Such measurements are done primarily using optical Faraday rotation in paraffin-coated cells [14–16,68] and recently also in the presence of buffer gas [32]. The duration of the probe pulse and the spatial profile of the probe beam determine the spatial profile of the squeezed spin state and hence its lifetime.

We shall employ the same two cells and geometry from the previous section [see Fig. 2(a)]. Given a probe pulse duration much shorter than w_0^2/D and assuming the measurement sensitivity surpasses the standard quantum limit, a squeezed state is formed, with initial spin variance $\langle \hat{x}_G^2(0) \rangle \leq 1/4$, where $\hat{x}_G(t)$ is the measured spin operator [defined in Appendix D as a weighted integral over the local operator $\hat{x}(\mathbf{r}, t)$]. The state is remeasured (validated) after some dephasing time t [see Fig. 3(a)]. In this type of experiments, narrow beams are often preferable, as the local intensity affects the measurement sensitivity, and since narrow beams simplify the use of optical cavities. Considering the different diffusion modes $u_n(\mathbf{r})$ with their decay rates Γ_n , we use Eq. (10) to calculate the evolution in the dark of the spin variance:

$$\langle \hat{x}_G^2(t) \rangle = \left(\sum_n |I_n^{(G)}|^2 e^{-\Gamma_n t} \right)^2 \left[\langle \hat{x}_G^2(0) \rangle - 1/4 \right] + 1/4. \quad (12)$$

Figures 3(b) and 3(c) present the calculated evolution. As expected, a narrow probe beam squeezes the atoms with which it overlaps, which are spanned in a superposition of diffusion modes [the first low-order modes in the buffer gas cell are visualized in Fig. 1(d)], leading to multimode temporal dynamics. The measured squeezing decreases due to atoms

diffusing out of the beam, as manifested by the exponential decay of each spatial mode. The importance of thermal motion grows as the degree of squeezing increases, as the latter relies on squeezing in higher-spatial modes. To see this, we plot in Fig. 3(d) the decay of squeezing in the buffer gas cell with a wide probe beam and with the initial state extremely squeezed ($\langle \hat{x}^2(\mathbf{r}, t=0) \rangle \ll 1/4$). The squeezing rapidly decays, as a power law, until only the lowest-order mode remains squeezed. This indicates the practical difficulty in achieving and maintaining a high degree of squeezing. An interesting behavior is apparent for the case of a large beam in a coated cell [Fig. 3(c), $w_0 = 8$ mm]. Here, the significant overlap with the uniform produces a certain degree of squeezing that is especially long lived.

These results demonstrate the significance of accounting for many diffusion modes when considering fragile non-classical states or high-fidelity operations. For example, the presented calculations for the 25-dB squeezing require 1000 modes to converge.

C. Coupling of alkali-metal spins to noble-gas spins

Lastly, we consider collisional spin exchange between two atomic species [2,7,33,35,36,39,69]. When the two species experience different wall couplings, their spin dynamics is determined by different diffusion-mode bases. Therefore mutual spin exchange, which is due to a local coupling (atom-atom collisions), depends on the mode overlap between these bases.

Here we consider the coupling of alkali-metal spins to noble-gas spins, such as helium-3, for potential applications in quantum optics [34]. The nuclear spins of noble gases are well protected by the enclosing complete electronic shells and thus sustain many collisions with other atoms and with the

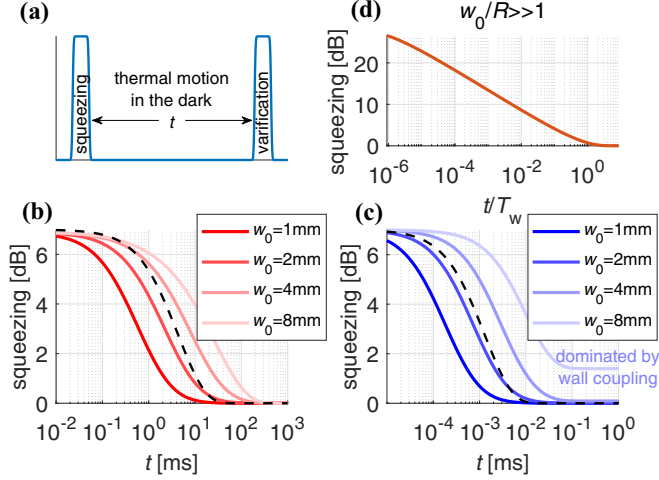


FIG. 3. Lifetime of spin squeezing. (a) Experimental sequence comprising a short measurement (squeezing) pulse, followed by dephasing in the dark due to thermal motion for duration t , and a verification pulse. The same probe beam is used for both pulses. In the calculations, the Gaussian distribution is initially squeezed by the measurement to spin variance of $\langle \hat{x}_G^2(0) \rangle = 0.05$ (7-dB squeezing). We take the same cell geometry as in Fig. 2 ($R = 1$ cm, $L = 3$ cm). (b) Degree of spin squeezing vs time in the buffer gas cell, calculated using Eq. (12). Spin squeezing exhibits multiexponential decay associated with multiple diffusion modes. Larger probe beams lead to longer squeezing lifetimes, as the beam overlaps better with lower-order modes. (c) Spin squeezing in the coated cell. In a coated cell, the decay rate of the uniform diffusion mode, dominated by wall coupling, is substantially lower than that of higher-order modes. Therefore, ensuring a significant overlap of the probe beam with the uniform mode is even more important in coated cells for maximizing the squeezing lifetime. The dotted line in (b) and (c) is a single exponential decay $\langle \hat{x}^2(t) \rangle = \langle \hat{x}^2(0) \rangle e^{-2\Gamma_w t} + (1 - e^{-2\Gamma_w t})/4$, shown for reference with $\Gamma_w = \pi^2 D/w_0^2$ and $w_0 = 4$ mm; note the difference in timescales between (b) and (c). (d) An extremely squeezed state relies more on higher-order spatial modes and thus loses its squeezing degree rapidly (time is normalized by $T_w = R^2/\pi^2 D$). The calculation is initialized with a uniform distribution of squeezing and includes the first 1000 radial modes, required for convergence.

cell walls. Their lifetime typically reaches minutes and hours [5,6,70]. In an alkali-metal-noble-gas mixture, the noble gas acts as a buffer both for itself and for the alkali-metal atoms, so that both species diffuse, and their collective spin states can be described by our Bloch-Heisenberg-Langevin model.

As the noble-gas spins do not relax by wall collisions, their lowest-order diffusion mode $u_n^b(\mathbf{r})$ is that associated with the characteristic (extremely) long lifetime. Higher-order modes $u_n^b(\mathbf{r})$ decay due to diffusion with typical rates $\Gamma_{\text{wall}} n^2 = n^2 \pi^2 D/R^2$, where R is the length scale of the system. For typical systems, Γ_{wall} is of the order of $(1 \text{ ms})^{-1} - (1 \text{ s})^{-1}$. Consequently, to enjoy the long lifetimes of noble-gas spins, one should employ solely the uniform mode.

The alkali-metal spins couple locally to the noble-gas spins with a collective rate J via spin-exchange collisions [33]. Unlike the noble-gas spins, the alkali-metal spins are strongly affected by the cell walls, and consequently their low-order diffusion modes $u_m^a(\mathbf{r})$ are different. This mode mismatch,

TABLE II. Overlap coefficients, $c_{mn} = \int_V d^3\mathbf{r} A_m^*(\mathbf{r}) B_n(\mathbf{r})$, of the first five spherically symmetric modes, i.e., $\ell = p = 0$. We take $A_m(\mathbf{r})$ to be the diffusion modes of a spherical cell with radius $R = 1$ and with destructive walls, and $B_n(\mathbf{r})$ to be the modes in the same cell but with spin-conserving walls.

c_{mn}	$n = 0$	$n = 1$	$n = 2$	$n = 3$	$n = 4$
$m = 0$	0.780	0.609	-0.126	0.058	-0.033
$m = 1$	-0.390	0.652	0.622	-0.158	0.079
$m = 2$	0.260	-0.274	0.647	0.627	-0.173
$m = 3$	-0.195	0.182	-0.256	0.644	0.629
$m = 4$	0.156	-0.139	0.1680	-0.246	0.643

between $u_m^a(\mathbf{r})$ and $u_n^b(\mathbf{r})$, leads to fractional couplings $c_{mn}J$, where $c_{mn} = \int_V d^3\mathbf{r} u_m^{a*}(\mathbf{r}) u_n^b(\mathbf{r})$ are the overlap coefficients. In particular, $|c_{m0}J|$ are the couplings to the uniform (long lived) mode of the noble-gas spins. Usually, no antirelaxation coating is used in these experiments, thus $|c_{m0}| < 1$.

Here we demonstrate a calculation for a spherical cell of radius R , for which the radial mode bases $u_m^a(\mathbf{r})$ and $u_n^b(\mathbf{r})$ and associated decay rates Γ_{am} and Γ_{bn} are presented in Appendix C, alongside the first c_{m0} values for an uncoated cell (Table II). The calculation includes the first $m, n \leq 70$ modes [71]. As the initial state, we consider the doubly excited (Fock) state of the alkali-metal spins $|\psi_0\rangle = \frac{1}{\sqrt{2}} (\sum_m \alpha_m a_m^\dagger)^2 |0\rangle_a |0\rangle_b = |2\rangle_a |0\rangle_b$, where $|0\rangle_a |0\rangle_b$ is the vacuum state with all spins pointing downwards. We take the initial excitation to be spatially uniform, for which the coefficients $\alpha_m = c_{m0}$ satisfy $\sum_m \alpha_m u_m(\mathbf{r}) = u_0^b(\mathbf{r}) = (4\pi R^3/3)^{-1/2}$. We calculate the transfer of this excitation via spin exchange to the uniform mode \hat{b}_0 of the noble-gas spins, i.e., to the state $|0\rangle_a |2\rangle_b = 2^{-1/2} (\hat{b}_0^\dagger)^2 |0\rangle_a |0\rangle_b$.

Figure 4 displays the exchange fidelity $\mathcal{F} = \max |\langle \psi(t) | 0\rangle_a |2\rangle_b|^2$ as a function of both spin-exchange rate J and quality of coating N . As N increases, the initial uniform excitation matches better the lower-order modes of the alkali-metal spins, which couple better to the uniform modes of the noble-gas spins. Indeed we find that the exchange fidelity grows with increasing J and N .

V. DISCUSSION

We have presented a fully quantum model, based on a Bloch-Heisenberg-Langevin formalism, for the effects of diffusion on the collective spin states in a thermal gas. The model is valid when the atomic mean free path is much shorter than the apparatus typical dimension. This is often the case for warm alkali-metal-vapor systems, even when a buffer gas is not deliberately introduced, as the out-gassing of a spin-preserving wall coating can lead to mean free paths on the order of millimeters [66,67].

We have mostly focused on highly polarized spin ensembles, typically used to study nonclassical phenomena that employ the transverse component of the spin. It is important to note that Eqs. (3) and (7) hold generally and can be applied to unpolarized systems as well. For example, the presented analysis of spin noise spectra holds for unpolarized vapor [accounting for suitable spin statistics in Eq. (11) using

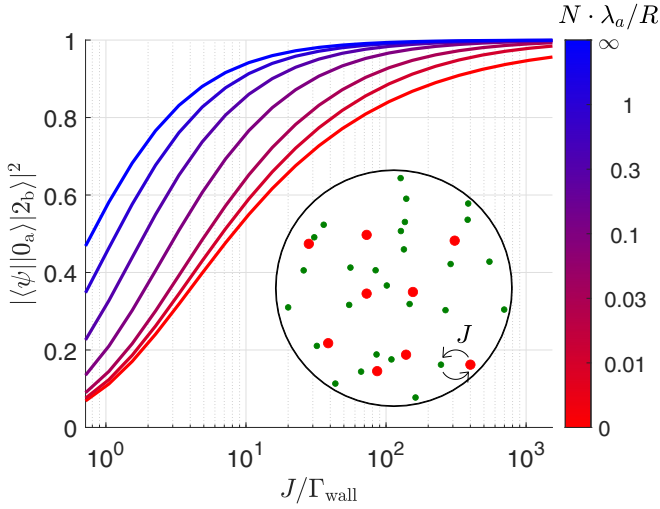


FIG. 4. Excitation exchange between polarized alkali-metal and noble-gas spins. Shown is the exchange fidelity of the doubly excited (Fock) states $|2\rangle_a|0\rangle_b$ and $|0\rangle_a|2\rangle_b$. We assume a spherical cell containing potassium and helium-3. The quality N of the wall coating for the alkali metal is varied between no coating ($N \leq 1$) and perfect coating ($N \rightarrow \infty$). The noble-gas spins do not couple to the cell walls. The exchange fidelity approaches 1 when $J \gg \Gamma_{\text{wall}}, \Gamma_a$, as then the spin exchange is efficient for many diffusion modes; here Γ_{wall} is the contribution of wall collisions to the relaxation rate of the alkali-metal spin (i.e., the typical diffusion rate to the walls), and Γ_a is the contribution of atomic collisions. The calculations are performed for a cell radius $R = 5$ mm and with 1 atm of helium-3. The diffusion constants are $D_a = 0.35$ cm²/s for the potassium (mean free path $\lambda_a = 50$ nm) so that $\Gamma_{\text{wall}} = \pi^2 D_a / R^2 = 1/(70$ ms), and $D_b = 0.7$ cm²/s for the helium (mean free path $\lambda_b = 20$ nm). The additional homogeneous decay of the alkali metal is $\Gamma_a \approx 6$ s⁻¹ [7]. The wall coating plays a significant role, since for $N\lambda_a/R > 1$ (i.e., $N > 10^5$) the diffusion modes of the potassium and helium spins match.

Eq. (D2)] and is thus applicable to nonclassical experiments done in that regime [32]. Our model can also describe other space-dependent phenomena, such as the dynamics in the presence of nonuniform driving fields [29].

The presented model agrees with existing mean-field descriptions of diffusion of atomic spins. It further agrees with models employing the dissipation-fluctuation theorem to derive the spin noise spectrum from the decay associated with diffusion. Importantly, it extends all these models by describing quantum correlations and explicitly deriving the quantum noise of the Brownian motion. The suggested model assumes $\lambda \ll R, L$ (Fickian diffusion) and thus does not hold for the special case of small, low-pressure, coated cells where the atomic motion is predominantly ballistic ($\lambda \gtrsim R, L$) [21,63]. Nevertheless, it may still provide a qualitative description of the effect of wall collisions on the uniform spin distribution across both diffusion regimes [63]. Our model lays the groundwork for treatments of such systems by considering non-Markovian motional dynamics.

Our results highlight the multimode nature of the dynamics. As exemplified for the applications considered in Sec. IV, one often needs to account for multiple diffusion modes, with

the high-order modes introducing additional quantum noise or reducing fidelities. As a rule of thumb, if ε is the allowed infidelity or excess quantum noise, then one should include the first $\approx \varepsilon^{-1}$ modes in the calculations.

Since thermal motion is inherent to gas-phase systems, our model could be beneficial to many studies of nonclassical spin gases and particularly to warm alkali-metal vapors. One such example is a recent demonstration of transfer of quantum correlations by the diffusion of alkali-metal atoms between different spatial regions [29]. Other examples involve a single active region, e.g., when spin squeezing is performed using a small probe beam over a long probing time, with the goal of coupling efficiently to the uniform diffusion mode in a coated cell [17,21]. The resulting spatiotemporal dynamics can be described using our model in order to assess the obtainable degree of squeezing. In particular, our model predicts that high buffer gas pressure would improve the lifetime of squeezed states when small probe beams are employed (e.g., when using optical cavities or when high probe intensities are needed), thus encouraging the realization of such experiments.

ACKNOWLEDGMENTS

We thank Eugene Polzik for fruitful discussions and insights. We acknowledge financial support by a European Research Council starting investigator grant (Q-PHOTONICS Grant No. 678674), the Israel Science Foundation, the Pazy Foundation, the Minerva Foundation with funding from the Federal German Ministry for Education and Research, and the Laboratory in Memory of Leon and Blacky Broder.

APPENDIX A: DIFFUSION-INDUCED NOISE

In the main text, we formulate the dynamics of a collective spin operator as driven from local density fluctuations. For deriving Eq. (3), we use the Lagrangian version of Eq. (2), where the noise is defined for each particle individually:

$$\partial n_a / \partial t = D \nabla^2 n_a + \nabla [\boldsymbol{\eta}^{(a)}(t) \sqrt{n_a}]. \quad (\text{A1})$$

Here $\boldsymbol{\eta}^{(a)}(t)$ is a white Gaussian process with vanishing mean $\langle \boldsymbol{\eta}^{(a)} \rangle_c = \mathbf{0}$ and with correlations $\langle \eta_i^{(a)}(t) \eta_j^{(a')}(t') \rangle_c = 2D \delta_{ij} \delta_{aa'} \delta(t - t')$. Substituting these into Eq. (1) provides the definition for the quantum noise components as

$$\hat{f}_\mu(\mathbf{r}, t) = \sum_{a=1}^{N_a} \hat{s}_\mu^{(a)}(t) \nabla [\boldsymbol{\eta}^{(a)} n_a(\mathbf{r}, t)]. \quad (\text{A2})$$

Following the lines of Ref. [47], we consider an alternative, equivalent definition

$$\hat{f}_\mu(\mathbf{r}, t) = \nabla [\hat{s}_\mu(\mathbf{r}, t) \boldsymbol{\eta}(\mathbf{r}, t) / \sqrt{n}], \quad (\text{A3})$$

as also provided in the main text. According to both definitions, \hat{f} is a stochastic Gaussian process (linear operations on a Gaussian process accumulate to a Gaussian process) with a vanishing mean. Consequently, the equivalence of the two definitions is a result of the equality of the noise

correlations:

$$\begin{aligned}
 \langle \hat{f}_\mu \hat{f}_\nu \rangle_c &= \left\langle \sum_i \nabla_i \left(\sum_a \hat{s}_\mu^{(a)} n_a \eta_i^{(a)} \right) \right. \\
 &\quad \times \left. \sum_j \nabla_j' \left(\sum_{a'} \hat{s}_\nu^{(a')} n_{a'} \eta_j^{(a')} \right) \right\rangle_c \\
 &= 2D(\nabla \cdot \nabla') \left(\sum_a \hat{s}_\mu^{(a)} \hat{s}_\nu^{(a)} n_a \right) \delta(\mathbf{r} - \mathbf{r}') \delta(t - t') \\
 &= 2D(\nabla \cdot \nabla') \frac{\sum_{aa'} \hat{s}_\mu^{(a)} \hat{s}_\nu^{(a')} n_a n_{a'}}{\sum_{a'} n_{a'}} \delta(\mathbf{r} - \mathbf{r}') \delta(t - t') \\
 &= 2D(\nabla \cdot \nabla') (\hat{s}_\mu \hat{s}'_\nu / \sqrt{nn'}) \delta(\mathbf{r} - \mathbf{r}') \delta(t - t') \\
 &= \left\langle \sum_i \nabla_i (\hat{s}_\mu \eta_i / \sqrt{n}) \times \sum_j \nabla_j' (\hat{s}'_\nu \eta_j' / \sqrt{n'}) \right\rangle_c, \quad (\text{A4})
 \end{aligned}$$

where we used the identity $n_a(\mathbf{r}, t) n_{a'}(\mathbf{r}, t) = \delta_{aa'} n_a(\mathbf{r}, t) n_{a'}(\mathbf{r}, t)$. Here and henceforth, we use tags to abbreviate the coordinates (\mathbf{r}', t') for a field, i.e., $F' = F(\mathbf{r}', t')$ and $F = F(\mathbf{r}, t)$.

The quantum noise, the commutation relations of which are shown in Eq. (4), conserves the spin commutation relations $[\hat{s}_\mu(\mathbf{r}, t), \hat{s}_\nu(\mathbf{r}', t)] = i\epsilon_{\xi\mu\nu} \hat{s}_\xi \delta(\mathbf{r} - \mathbf{r}')$. This can be seen from

$$\begin{aligned}
 &[\hat{s}_\mu(\mathbf{r}, t + dt), \hat{s}_\nu(\mathbf{r}', t + dt)] - [\hat{s}_\mu(\mathbf{r}, t), \hat{s}_\nu(\mathbf{r}', t)]_c \\
 &= i\epsilon_{\xi\mu\nu} \delta(\mathbf{r} - \mathbf{r}') (\hat{s}_\xi(\mathbf{r}, t + dt) - \hat{s}_\xi(\mathbf{r}, t))_c \quad (\text{A5})
 \end{aligned}$$

and then

$$\begin{aligned}
 &i\epsilon_{\xi\mu\nu} D(\nabla + \nabla')^2 [\hat{s}_\xi \delta(\mathbf{r} - \mathbf{r}')] dt \\
 &= i\epsilon_{\xi\mu\nu} D(\nabla^2 \hat{s}_\xi) \delta(\mathbf{r} - \mathbf{r}') dt, \quad (\text{A6})
 \end{aligned}$$

where the last equality stems from $(\nabla + \nabla')\delta(\mathbf{r} - \mathbf{r}') = 0$.

In Sec. III, we focus on highly polarized ensembles, where the dynamics is described by the bosonic annihilation operator \hat{a} , under the Holstein-Primakoff approximation. Under these conditions, the thermal noise operating on the bosonic excitations becomes $\hat{f} = \nabla(\hat{a}\eta/\sqrt{n})$. In addition, the same conditions ensure that $\hat{a}^\dagger \hat{a} = 0$, $\hat{a}(\mathbf{r}, t) \hat{a}^\dagger(\mathbf{r}', t) = \delta(\mathbf{r} - \mathbf{r}')$, and $\hat{a}(\mathbf{r}, t) \hat{a}^\dagger(\mathbf{r}', t) \delta(\mathbf{r} - \mathbf{r}') = n\delta(\mathbf{r} - \mathbf{r}')$, thus providing

$$\begin{aligned}
 \langle \hat{f} \hat{f}'^\dagger \rangle_c &= \langle \nabla \hat{a} \eta / \sqrt{n} \nabla' (\hat{a}^\dagger)' \eta' / \sqrt{n'} \rangle_c \\
 &= -2D \nabla^2 \delta(\mathbf{r} - \mathbf{r}') \delta(t - t'), \quad (\text{A7})
 \end{aligned}$$

and $\langle \hat{f}^\dagger \hat{f}' \rangle_c = 0$. Therefore, the noise becomes a vacuum noise and conserves the commutation relations of the bosonic operators. We denote the correlations of the diffusion noise in the bulk as $C(\mathbf{r}, \mathbf{r}') = -2D \nabla^2 \delta(\mathbf{r} - \mathbf{r}')$.

APPENDIX B: MODEL FOR WALL COUPLING

We adopt a simplified model for describing the scattering of atoms off the cell walls. The model assumes that the wall coupling is stochastic and Markovian, thus resulting in an exponential decay of the scattered spin, and that the noise due to diffusion in the bulk vanishes within a thin boundary layer at the wall. This leads to the scattering described by Eq. (6). The accompanying noise processes for atoms a and a' satisfy

the relations

$$[\hat{w}_a^\mu(t), \hat{w}_{a'}^\nu(t')] = i\epsilon_{\mu\nu\xi} e^{-1/N} (1 - e^{-1/N}) \hat{s}_\xi^{(a)} \delta_{aa'} \frac{\varpi \delta(t - t')}{\bar{v}}, \quad (\text{B1})$$

where $\mu, \nu = x, y, z$. Here $\varpi = (e^{1/N} - 1)^{-1} \lambda/3$ is the effective correlation distance of the wall-scattering noise, defined such that the commutation relations of the spin operators are conserved for all diffusion modes, i.e., for the entire cell (bulk and boundary). It changes monotonically from $\varpi = e^{-1/N} \lambda/3$ for spin-destructing walls ($N \ll 1$) to $\varpi = N\lambda/3$ for spin-preserving walls ($N \gg 1$).

The continuous operator $\hat{w}(\mathbf{r}, t)$ used in the main text to describe the noise due to interactions with the cell walls is defined as $\hat{w} = \sum_a \hat{w}_a n_a$. It is the analog of $\hat{w}_a(t)$, like \hat{s} is to \hat{s}_a . It vanishes for positions \mathbf{r} the distance of which from the boundary is larger than ϖ , and its commutation relations are

$$\begin{aligned}
 \langle [\hat{w}^\mu, \hat{w}'^\nu] \rangle_c &= i\epsilon_{\mu\nu\xi} e^{-1/N} (1 - e^{-1/N}) \varpi / \bar{v} \\
 &\quad \times \hat{s}_\xi(\mathbf{r}, t) \delta(\mathbf{r} - \mathbf{r}') \delta(t - t'). \quad (\text{B2})
 \end{aligned}$$

The last expression is defined only for coordinates \mathbf{r} and \mathbf{r}' on the cell boundary and vanishes elsewhere. As an example, for a rectangular cell with a wall at $x = L/2$, we shall define coordinates on the boundary $\mathbf{r}_\perp = y\hat{y} + z\hat{z}$ and substitute $\delta(\mathbf{r} - \mathbf{r}') = \frac{1}{\varpi} \delta(y - y') \delta(z - z')$ at $x = x' = L/2$. For a spherical cell with a wall at $|\mathbf{r}| = R$, we use $\delta(\mathbf{r} - \mathbf{r}') = \frac{1}{\varpi} \frac{\delta(\Omega - \Omega')}{R^2}$, where Ω is the angular position of coordinate \mathbf{r} .

Using $\hat{w}(\mathbf{r}, t)$, the scattering matrix for the spin-density operator becomes $\mathcal{S}\hat{s} = e^{-1/N} \cdot \hat{s} + \hat{w}$. We write Eq. (7) for the spin-density operator using the noise field \hat{w} . In addition, \hat{w} is defined only on the boundary, such that $(\hat{\mathbf{n}} \cdot \nabla) \hat{w}|_{\text{boundary}} \propto \delta'(0)$ and therefore vanishes.

Finally, under the Holstein-Primakoff approximation, we use Eq. (B2) to find the noise operating on \hat{a} due to wall scattering. The operator $\hat{w} = \hat{w}_- / \sqrt{2} |s_z\rangle$ becomes a vacuum noise, satisfying $\langle \hat{w}^\dagger \hat{w}' \rangle_c = 0$, and for \mathbf{r} and \mathbf{r}' on the cell boundary

$$\langle \hat{w} \hat{w}'^\dagger \rangle_c = 2e^{-1/N} (1 - e^{-1/N}) \varpi / \bar{v} \delta(\mathbf{r} - \mathbf{r}') \delta(t - t'). \quad (\text{B3})$$

Considering a general spin distribution, the noise due to the walls exists only in a volume of order ϖS , where S is the cell surface area, while the noise due to diffusion in the bulk exists in the entire volume V . The ratio of the two scales as $\langle \hat{w} \hat{w}'^\dagger \rangle_c / \langle \hat{f} \hat{f}'^\dagger \rangle_c \propto \varpi S / V \propto \lambda / R$, where R is the typical dimension of the cell. Consequently, in our considered diffusive regime $\lambda \ll R$, the diffusion noise dominates over that of the wall scattering for nonuniform spin distributions.

APPENDIX C: SOLVING THE DIFFUSION-RELAXATION BLOCH-HEISENBERG-LANGEVIN EQUATIONS

The diffusion-relaxation equation in the Bloch-Heisenberg-Langevin formalism, in the limit of a highly polarized spin gas, is presented in Sec. III. Here we first solve Eqs. (8) and (9) for a simplified 1D case by following the method described in the main text. We provide explicit expressions for the mode-specific noise sources due to motion in the bulk and at the boundary. Finally, we provide tabulated

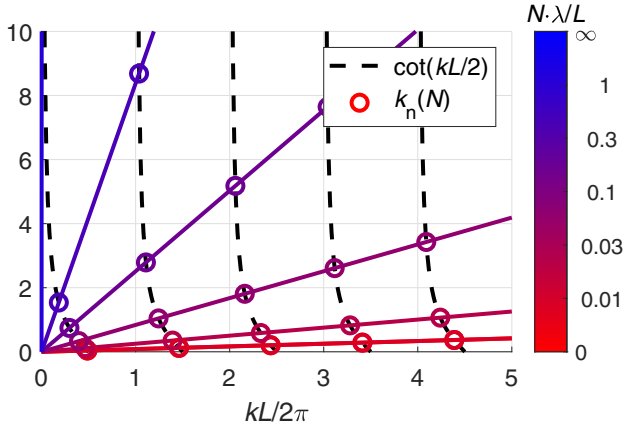


FIG. 5. Graphical solutions for the Robin boundary condition. Here we solve the 1D equations for a system of length $L = 1$ cm and mean free path of $\lambda = 0.5 \mu\text{m}$ (characteristic of 100 Torr of buffer gas) and for different values of N .

solutions for the three-dimensional cases of rectangular, cylindrical, and spherical cells.

Consider a 1D cell with a single spatial coordinate $-L/2 \leq x \leq L/2$. The functions $u_k(x)$ that solve the Helmholtz equation $\partial^2 u_k / \partial x^2 + k^2 u_k = 0$ are the relaxation-diffusion modes, where the decay rates Γ introduced in the main text are $\Gamma = Dk^2$. These solutions are $u_k^+ = A_k^+ \cos(k^+ x)$ and $u_k^- = A_k^- \sin(k^- x)$, composing symmetric and antisymmetric modes. The annihilation operator decomposes into a superposition $\hat{a}(x, t) = \sum_{k, \pm} \hat{a}_k^\pm(t) u_k^\pm(x)$. To further simplify the example, we take only symmetric spin distribution and symmetric noise into consideration, i.e., we keep only the modes u_k^+ and omit the “+” superscript. Note that a physical noise is random and generally has no defined symmetry, but it can be decomposed into components with well-defined symmetry.

The bulk diffusion equation becomes $\partial \hat{a}_k / \partial t = i[\mathcal{H}, \hat{a}_k] - Dk^2 \hat{a}_k + \int_{-L/2}^{L/2} \hat{f} u_k dx$. We break the boundary equation into a homogeneous part, where the noise is omitted, and an inhomogeneous part, which includes the noise. The former can be decomposed into the different modes and is simplified to the algebraic equation $\cot(kL/2) = 2 \frac{1+e^{-1/N}}{1-e^{-1/N}} \lambda k$ [72].

For general values of N , this is a Robin boundary condition, which can be solved numerically or graphically as presented in Fig. 5. The discrete solutions k_n define a complete and orthonormal set of discrete modes $u_n = A_n \cos(k_n x)$, spanning all symmetric spin distributions in the 1D cell, and $\int_{-L/2}^{L/2} u_m^* u_n dx = \delta_{nm}$. These provide the discrete decay rates Γ_n .

For example, in the Dirichlet case of destructive walls ($N\lambda/L \ll 1$), $k_n = (2n+1)\pi/L$. The annihilation operators of the various modes are $\hat{a}_n(t) = \int_{-L/2}^{L/2} u_n^*(x) \hat{a}(x, t) dx$, and the noise operators are $\hat{f}_n(t) = \int_{-L/2}^{L/2} u_n^*(x) \hat{f}(x, t) dx$ and $\hat{w}(t) = [\hat{w}(L/2, t) + \hat{w}(-L/2, t)]/2$.

The treatment of \hat{f}_n as a bulk source term operating on independent modes is a common technique [73]. It differs, however, from the treatment of the noise at the boundaries.

We deal with this term by defining auxiliary fields

$$\hat{a}(x, t) = \hat{p}(x, t) + \sum_n \hat{h}_n(t) u_n(x), \quad (C1)$$

as we desire to use $\hat{p}(x, t)$ to imbue the wall noise as a source acting on the modes \hat{a}_n , while \hat{h}_n solves the homogeneous equations in the absence of wall-induced fluctuations. Therefore $\hat{p}(x, t)$ is defined such that $\nabla^2 \hat{p}(x, t) = 0$.

In our 1D symmetric case, $\hat{p}(x, t) = \hat{p}(t)$ is uniform. Writing the full boundary equation for \hat{a} provides $\hat{p}(t) = \hat{w}(t)/(1 - e^{-1/N})$. We decompose $\hat{p}(t)$ into the modes to obtain $\hat{p}_n(t) = \int_{-L/2}^{L/2} \hat{p}(t) u_n(x) dx = 2A_n \sin(k_n L/2) \hat{p}(t)/k_n$. Substituting this in Eq. (8) provides the equation for the homogeneous mode operators \hat{h}_n .

In the case of a magnetic Zeeman Hamiltonian $\mathcal{H} = i\omega_0 \hat{S}_z$, we find

$$\partial \hat{h}_n / \partial t = -i\omega_0 \hat{h}_n - \Gamma_n \hat{h}_n + \hat{f}_n - i\omega_0 \hat{p}_n - \partial \hat{p}_n / \partial t, \quad (C2)$$

the solutions of which are

$$\hat{h}_n = e^{-(i\omega_0 + \Gamma_n)t} \hat{h}_n(0) + \int_0^t e^{-(i\omega_0 + \Gamma_n)(t-\tau)} [\hat{f}_n(\tau) - (i\omega_0 + \frac{\partial}{\partial \tau}) \hat{p}_n(\tau)] d\tau. \quad (C3)$$

Substituting into $\hat{a}_n(t) = \hat{p}_n(t) + \hat{h}_n(t)$ and differentiating with respect to t provides the evolution of the annihilation operators of the spin modes

$$\partial \hat{a}_n / \partial t = -(i\omega_0 + \Gamma_n) \hat{a}_n + \hat{f}_n + \hat{f}_n^w, \quad (C4)$$

where

$$\hat{f}_n^w = \Gamma_n \int_{-L/2}^{L/2} u_n^*(x) \hat{p}(x, t) dx = \frac{2A_n \Gamma_n \sin(k_n L/2)}{(1 - e^{-1/N}) k_n} \hat{w} \quad (C5)$$

is the quantum noise due to wall collisions. Finally, we can combine the two noise terms and obtain the total, mode-specific, noise operator

$$\hat{\mathcal{W}}_n = \int_0^t e^{-[i\omega_0 + D(k_n^\pm)^2](t-\tau)} [\hat{f}_n(\tau) + \hat{f}_n^w(\tau)] d\tau, \quad (C6)$$

appearing in Eq. (10).

Under the influence of the noise sources $\hat{\mathcal{W}}_n$ and the dissipation Γ_n , the spin operators of the diffusion modes obey the fluctuation-dissipation theorem, and their commutation relations are conserved, resulting from $\langle (\hat{f}_n + \hat{f}_n^w)(\hat{f}_n + \hat{f}_n^w)^\dagger \rangle_c = 2\Gamma_n \delta_{nn} \delta(t-t')$ and $\langle (\hat{f}_n + \hat{f}_n^w)^\dagger (\hat{f}_n + \hat{f}_n^w) \rangle_c = 0$. Note that the conservation of local commutation relations is already presented in Appendices A and B (where \hat{f} applies for the bulk and \hat{w} for the boundary) without the mode decomposition. Notably, however, it also holds for the nonlocal (diffusion) modes.

For completeness, we provide in Table I the diffusion-relaxation modes for rectangular, cylindrical, and spherical cells. Various applications, such as those involving collisional (local) coupling between two spin ensembles, also require the overlap coefficients $c_{mn} = \int_V d^3 \mathbf{r} A_m^*(\mathbf{r}) B_n(\mathbf{r})$ between diffusion modes $A_m(\mathbf{r})$ and $B_n(\mathbf{r})$. These are presented in Table II for spherically symmetric modes, where $A_m(\mathbf{r})$ are modes for highly destructive walls ($N \lesssim 1$), and $B_n(\mathbf{r})$ are for inert walls ($N \gg L/\lambda$). These conditions are typical for a mixture of alkali-metal vapor and noble gas, as discussed in Sec. IV.

APPENDIX D: FARADAY ROTATION MEASUREMENT SETUP

In Sec. IV, we consider two experimental setups where the transverse component of a polarized spin ensemble is measured by means of the Faraday rotation. This scheme is common in alkali-metal spin measurements [14,32,74,75]. As illustrated in Fig. 2(a), we consider a cylindrical cell with radius R and length L , with the cylinder axis along $\hat{\mathbf{x}}$. The spins are polarized along $\hat{\mathbf{z}}$, parallel to an external applied magnetic field $\mathbf{B} = B\hat{\mathbf{z}}$. We use ρ and φ as the cylindrical coordinates, and x as the axial coordinate.

A linearly polarized probe beam travels along $\hat{\mathbf{x}}$ with a Gaussian intensity profile $I_G(\mathbf{r}) = I_0 \exp(-2\rho^2/w_0^2)$, where w_0 is the beam waist radius. We assume a negligible beam divergence within the cell and require the normalization $\int_V I_G^2(\mathbf{r}) d^3\mathbf{r} = 1$, so that $(I_0)^{-2} = \pi L w_0^2 (1 - e^{-4R^2/w_0^2})/4$. The probe frequency is detuned from the atomic transition, such that the probe is not depleted and does not induce additional spin decay.

The linear polarization of the probe rotates due to the Faraday effect, with the rotation angle proportional to the spin projection along the beam propagation direction. Therefore, measurement of the rotation angle provides a measurement of \hat{s}_x weighted by its overlap with the beam profile. Precisely, the operator $\hat{x}_G(t) = \int_V d^3\mathbf{r} I_G(\mathbf{r}) \hat{x}(\mathbf{r}, t)$, where $\hat{x}(\mathbf{r}, t) = [\hat{a}(\mathbf{r}, t) + \hat{a}^\dagger(\mathbf{r}, t)]/2$, is measured in this scheme [17].

We identify the atomic diffusion modes in the cylindrical cell as $u_n(\mathbf{r})$. Note that in Table I the modes require several labels, which we replace here with a single label n for brevity. We decompose the spin operator and the probe intensity profile using the modes $\hat{x}(\mathbf{r}, t) = \sum_n \hat{x}_n(t) u_n(\mathbf{r})$ and $I_G(\mathbf{r}) = \sum_n I_n^{(G)} u_n(\mathbf{r})$, where $\hat{x}_n(t) = (\hat{a}_n + \hat{a}_n^\dagger)/2$ and $I_n^{(G)} = \int_V d^3\mathbf{r} I_G(\mathbf{r}) u_n^*(\mathbf{r})$. Using these, we express the measured spin operator as $\hat{x}_G(t) = \sum_n I_n^{(G)} \hat{x}_n(t)$.

We calculate the spin noise spectrum from its formal definition

$$S_{xx}(f) = \lim_{T \rightarrow \infty} \frac{1}{T} \int_0^T \int_0^T \hat{x}_G(\tau) \hat{x}_G(\tau') e^{2\pi i f(\tau - \tau')} d\tau d\tau' \quad (\text{D1})$$

utilizing the temporal evolution of the modes as given by Eq. (10), and including the noise properties $\hat{\mathcal{W}}_n^\dagger(t) \hat{\mathcal{W}}_n(t) = 0$ and $\hat{\mathcal{W}}_n(t) \hat{\mathcal{W}}_n^\dagger(t) = (1 - e^{-2\Gamma_n t}) \delta_{n'n}$ derived from Appendix C. The spin noise spectral density appearing in Eq. (11) holds for both polarized and unpolarized ensembles, with

$$\tilde{P} = \begin{cases} 1 & \text{polarized} \\ 2(S+1)/3 & \text{unpolarized} \end{cases} \quad (\text{D2})$$

where S is the single-particle spin magnitude.

For the considered geometry, the standard quantum limit is $\langle \hat{S}_x^2 \rangle \geq N_{\text{beam}}/4 = \frac{nV_{\text{beam}}}{4} \frac{[1 - \exp(-2R^2/w_0^2)]^2}{1 - \exp(-4R^2/w_0^2)}$, where $N_{\text{beam}} = n[\int_V I_G(\mathbf{r}) d^3r]^2 / \int_V I_G^2(\mathbf{r}) d^3r$ is the number of atoms in the beam, and $V_{\text{beam}} = \pi L w_0^2$ is the beam volume [76].

-
- [1] W. Happer, *Rev. Mod. Phys.* **44**, 169 (1972).
 [2] W. Happer and A. C. Tam, *Phys. Rev. A* **16**, 1877 (1977).
 [3] O. Katz and O. Firstenberg, *Nat. Commun.* **9**, 2074 (2018).
 [4] M. V. Balabas, T. Karaulanov, M. P. Ledbetter, and D. Budker, *Phys. Rev. Lett.* **105**, 070801 (2010).
 [5] T. G. Walker and W. Happer, *Rev. Mod. Phys.* **69**, 629 (1997).
 [6] T. R. Gentile, P. J. Nacher, B. Saam, and T. G. Walker, *Rev. Mod. Phys.* **89**, 045004 (2017).
 [7] W. Happer, Y.-Y. Jau, and T. Walker, *Optically Pumped Atoms* (Wiley, New York, 2010).
 [8] J. M. Brown, S. J. Smullin, T. W. Kornack, and M. V. Romalis, *Phys. Rev. Lett.* **105**, 151604 (2010).
 [9] D. Sheng, S. Li, N. Dural, and M. V. Romalis, *Phys. Rev. Lett.* **110**, 160802 (2013).
 [10] D. Budker and M. Romalis, *Nat. Phys.* **3**, 227 (2007).
 [11] D. Budker and D. F. J. Kimball, *Optical Magnetometry* (Cambridge University, Cambridge, England, 2013).
 [12] S. A. Crooker, D. G. Rickel, A. V. Balatsky, and D. L. Smith, *Nature (London)* **431**, 49 (2004).
 [13] I. M. Bloch, Y. Hochberg, E. Kuflik, and T. Volansky, *J. High Energy Phys.* **01** (2020) 167.
 [14] B. Julsgaard, A. Kozhekin, and E. S. Polzik, *Nature (London)* **413**, 400 (2001).
 [15] J. F. Sherson, H. Krauter, R. K. Olsson, B. Julsgaard, K. Hammerer, I. Cirac, and E. S. Polzik, *Nature (London)* **443**, 557 (2006).
 [16] K. Jensen, W. Wasilewski, H. Krauter, T. Fernholz, B. M. Nielsen, M. Owari, M. B. Plenio, A. Serafini, M. M. Wolf, and E. S. Polzik, *Nat. Phys.* **7**, 13 (2011).
 [17] K. Hammerer, A. S. Sørensen, and E. S. Polzik, *Rev. Mod. Phys.* **82**, 1041 (2010).
 [18] M. D. Eisaman, A. André, F. Massou, M. Fleischhauer, A. S. Zibrov, and M. D. Lukin, *Nature (London)* **438**, 837 (2005).
 [19] T. Peyronel, O. Firstenberg, Q.-Y. Liang, S. Hofferberth, A. V. Gorshkov, T. Pohl, M. D. Lukin, and V. Vuletić, *Nature (London)* **488**, 57 (2012).
 [20] A. V. Gorshkov, J. Otterbach, M. Fleischhauer, T. Pohl, and M. D. Lukin, *Phys. Rev. Lett.* **107**, 133602 (2011).
 [21] J. Borregaard, M. Zugenmaier, J. M. Petersen, H. Shen, G. Vasilakis, K. Jensen, E. S. Polzik, and A. S. Sørensen, *Nat. Commun.* **7**, 11356 (2016).
 [22] A. Kastler, *J. Opt. Soc. Am.* **47**, 460 (1957).
 [23] F. Masnou-Seeuws and M.-A. Bouchiat, *J. Phys.* **28**, 406 (1967).
 [24] Z. Wu, S. Schaefer, G. D. Cates, and W. Happer, *Phys. Rev. A* **37**, 1161 (1988).
 [25] S. Li, P. Vachaspati, D. Sheng, N. Dural, and M. V. Romalis, *Phys. Rev. A* **84**, 061403(R) (2011).
 [26] O. Firstenberg, M. Shuker, A. Ben-Kish, D. R. Fredkin, N. Davidson, and A. Ron, *Phys. Rev. A* **76**, 013818 (2007).
 [27] O. Firstenberg, P. London, D. Yankelev, R. Pugatch, M. Shuker, and N. Davidson, *Phys. Rev. Lett.* **105**, 183602 (2010).
 [28] Y. Xiao, I. Novikova, D. F. Phillips, and R. L. Walsworth, *Phys. Rev. Lett.* **96**, 043601 (2006).
 [29] J. Sun, X. Zhang, W. Qu, E. E. Mikhailov, I. Novikova, H. Shen, and Y. Xiao, *Phys. Rev. Lett.* **123**, 203604 (2019).
 [30] H. Bao, J. Duan, S. Jin, X. Lu, P. Li, W. Qu, M. Wang, I. Novikova, E. E. Mikhailov, K.-F. Zhao *et al.*, *Nature (London)* **581**, 159 (2020).

- [31] H. Bao, M. Wang, P. Li, W. Qu, E. Mikhailov, I. Novikova, H. Shen, and Y. Xiao, in *2016 Proceedings of Progress in Electromagnetic Research Symposium (PIERS)* (IEEE, 2016), p. 3974.
- [32] J. Kong, R. Jiménez-Martínez, C. Troullinou, V. G. Lucivero, G. Tóth, and M. W. Mitchell, *Nat. Commun.* **11**, 2415 (2020).
- [33] O. Katz, R. Shaham, and O. Firstenberg, [arXiv:1905.12532v2](https://arxiv.org/abs/1905.12532v2).
- [34] O. Katz, R. Shaham, E. S. Polzik, and O. Firstenberg, *Phys. Rev. Lett.* **124**, 043602 (2020).
- [35] A. T. Dellis, M. Loulakis, and I. K. Komínis, *Phys. Rev. A* **90**, 032705 (2014).
- [36] K. Mouloudakis, M. Loulakis, and I. K. Komínis, *Phys. Rev. Research* **1**, 033017 (2019).
- [37] K. Mouloudakis and I. K. Komínis, [arXiv:2004.11790v2](https://arxiv.org/abs/2004.11790v2).
- [38] G. Vasilakis, V. Shah, and M. V. Romalis, *Phys. Rev. Lett.* **106**, 143601 (2011).
- [39] D. Roy, L. Yang, S. A. Crooker, and N. A. Sinitsyn, *Sci. Rep.* **5**, 9573 (2015).
- [40] S. Seltzer and M. V. Romalis, *J. Appl. Phys.* **106**, 114905 (2009).
- [41] V. G. Lucivero, N. D. McDonough, N. Dural, and M. V. Romalis, *Phys. Rev. A* **96**, 062702 (2017).
- [42] N. A. Sinitsyn and Y. V. Pershin, *Rep. Prog. Phys.* **79**, 106501 (2016).
- [43] G. E. Katsoprinakis, A. T. Dellis, and I. K. Komínis, *Phys. Rev. A* **75**, 042502 (2007).
- [44] P. Glasenapp, N. A. Sinitsyn, L. Yang, D. G. Rickel, D. Roy, A. Greulich, M. Bayer, and S. A. Crooker, *Phys. Rev. Lett.* **113**, 156601 (2014).
- [45] V. G. Lucivero, R. Jiménez-Martínez, J. Kong, and M. W. Mitchell, *Phys. Rev. A* **93**, 053802 (2016).
- [46] V. G. Lucivero, A. Dimic, J. Kong, R. Jiménez-Martínez, and M. W. Mitchell, *Phys. Rev. A* **95**, 041803(R) (2017).
- [47] D. S. Dean, *J. Phys. A* **29**, L613 (1996).
- [48] C. H. Volk, J. G. Mark, and B. C. Grover, *Phys. Rev. A* **20**, 2381 (1979).
- [49] T. M. Kwon, J. G. Mark, and C. H. Volk, *Phys. Rev. A* **24**, 1894 (1981).
- [50] P. A. Heimann, I. A. Greenwood, and J. H. Simpson, *Phys. Rev. A* **23**, 1209 (1981).
- [51] Z. Wu, W. Happer, and J. M. Daniels, *Phys. Rev. Lett.* **59**, 1480 (1987).
- [52] E. B. Alexandrov, M. V. Balabas, D. Budker, D. English, D. F. Kimball, C. H. Li, and V. V. Yashchuk, *Phys. Rev. A* **66**, 042903 (2002).
- [53] M. T. Graf, D. F. Kimball, S. M. Rochester, K. Kerner, C. Wong, D. Budker, E. B. Alexandrov, M. V. Balabas, and V. V. Yashchuk, *Phys. Rev. A* **72**, 023401 (2005).
- [54] B. Driehuys, G. D. Cates, W. Happer, H. Mabuchi, B. Saam, M. S. Albert, and A. Wishnia, *Phys. Lett. A* **184**, 88 (1993).
- [55] B. Driehuys, G. D. Cates, and W. Happer, *Phys. Rev. Lett.* **74**, 4943 (1995).
- [56] S. R. Breeze, S. Lang, I. Moudrakovski, C. I. Ratcliffe, J. A. Ripmeester, B. Simard, and G. Santyr, *J. Appl. Phys.* **86**, 4040 (1999).
- [57] M. F. Hsu, G. D. Cates, I. Komínis, I. A. Aksay, and D. M. Dabbs, *Appl. Phys. Lett.* **77**, 2069 (2000).
- [58] For long-lived solutions of the diffusion equation, the flux towards the wall $\hat{n} \cdot \nabla \hat{s}$ is of the same order as \hat{s}/R .
- [59] This limit is obtained only when $\lambda \ll R$, which is also necessary for the validity of the diffusion equation.
- [60] M. N. Ozisik, *Boundary Value Problems of Heat Conduction* (Courier, New York, 2002).
- [61] T. Holstein and H. Primakoff, *Phys. Rev.* **58**, 1098 (1940).
- [62] C. Kittel, *Quantum Theory of Solids* (John Wiley & Sons, New York, 1987).
- [63] Y. Tang, Y. Wen, L. Cai, and K. Zhao, *Phys. Rev. A* **101**, 013821 (2020).
- [64] M. C. D. Tayler, T. F. Sjolander, A. E. Pines, and D. Budker, *J. Magn. Reson.* **270**, 35 (2016).
- [65] R. Pugatch, O. Firstenberg, M. Shuker, and N. Davidson, *Phys. Rev. Lett.* **102**, 150602 (2009).
- [66] N. Sekiguchi and A. Hatakeyama, *Appl. Phys. B* **122**, 81 (2016).
- [67] A. Hatakeyama, T. Kuroda, N. Sekiguchi, and K. Ishikawa, *Appl. Phys. B* **125**, 133 (2019).
- [68] W. Wasilewski, K. Jensen, H. Krauter, J. J. Renema, M. V. Balabas, and E. S. Polzik, *Phys. Rev. Lett.* **104**, 133601 (2010).
- [69] O. Katz, O. Peleg, and O. Firstenberg, *Phys. Rev. Lett.* **115**, 113003 (2015).
- [70] C. Gemmel, W. Heil, S. Karpuk, K. Lenz, C. Ludwig, Y. Sobolev, K. Tullney, M. Burghoff, W. Kilian, S. Knappe-Grüneberg, W. Müller, A. Schnabel, F. Seifert, L. Trahms, and S. Baeßler, *Eur. Phys. J. D* **57**, 303 (2010).
- [71] Excess decay and noise due to the modes $m, n \geq 70$ are introduced along the lines of Eq. (S4) in Ref. [33].
- [72] Here in one dimension, we use the relation $D = \lambda \bar{v}$ between the diffusion coefficient and the kinetic parameters. In three dimensions, this becomes $D = \lambda \bar{v}/3$, such that $\cot(kL/2) = \frac{2}{3} \frac{1+e^{-1/N}}{1-e^{-1/N}} \lambda k$. ϖ has similar dimensionality dependence.
- [73] D. A. Steck, *Quantum and Atom Optics* (Department of Physics, University of Oregon, Eugene, Oregon, 2007).
- [74] V. B. Braginsky and F. Y. Khalili, *Rev. Mod. Phys.* **68**, 1 (1996).
- [75] S. Appelt, A. B. Baranga, C. J. Erickson, M. V. Romalis, A. R. Young, and W. Happer, *Phys. Rev. A* **58**, 1412 (1998).
- [76] V. Shah, G. Vasilakis, and M. V. Romalis, *Phys. Rev. Lett.* **104**, 013601 (2010).